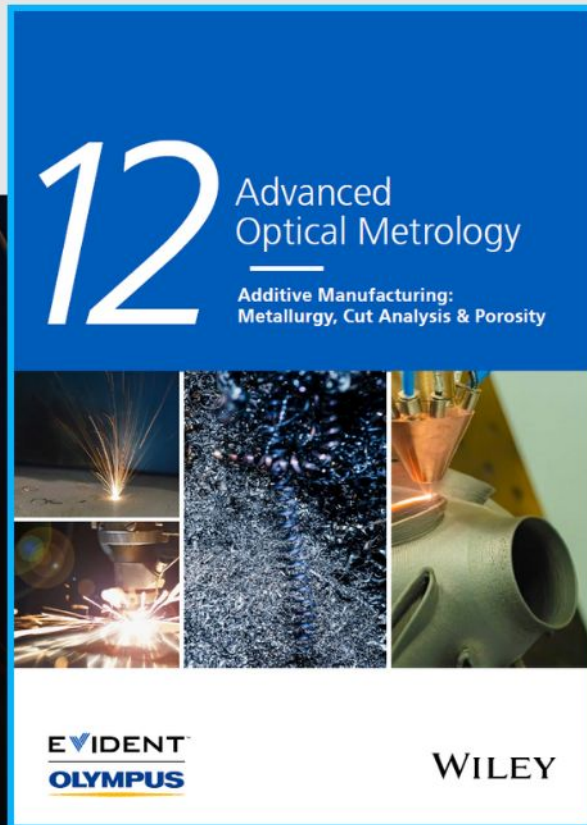




Additive Manufacturing: Metallurgy, Cut Analysis & Porosity

The latest eBook from
Advanced Optical Metrology.
Download for free.



In industry, sector after sector is moving away from conventional production methods to additive manufacturing, a technology that has been recommended for substantial research investment.

Download the latest eBook to read about the applications, trends, opportunities, and challenges around this process, and how it has been adapted to different industrial sectors.

EVIDENT
OLYMPUS

WILEY

Application limits and sensitisation behaviour of the manganese- and nitrogen-alloyed austenitic stainless steel P2000 (X13CrMnMoN18-14-3)

Norman Kauss^{1,2}  | Andreas Heyn¹  | Oliver Michael¹ | Michael Schymura³ | Paul Rosemann^{1,4}

¹Institute of Materials and Joining Technology, Otto-von-Guericke University Magdeburg, Magdeburg, Germany

²Division 7.6 Corrosion and Corrosion Protection, Federal Institute for Materials Research and Testing (BAM), Berlin, Germany

³Department of High Nitrogen Steels, Research & Development, Energietechnik Essen GmbH, Essen, Germany

⁴Institute for Technology and Production in Mechanical Engineering, HTWK Leipzig University of Applied Sciences, Leipzig, Germany

Correspondence

Norman Kauss, Institute of Materials and Joining Technology, Otto-von-Guericke University 39106, Magdeburg, Germany. Email: Norman.Kauss@ovgu.de

Funding information

Deutsche Forschungsgemeinschaft, Grant/Award Number: 330472124

Abstract

Nickel-free high-nitrogen-alloyed stainless steels like the P2000 (X13CrMnMoN18-14-3) were developed to enhance the strength and corrosion resistance of austenitic stainless steels like 304 and 316 while keeping the typical high ductility. The mechanical and corrosive properties of P2000 were investigated and compared with 304 and 316 to highlight the application opportunities of this new alloy. The microstructure of the solution-annealed condition was characterised by electron backscatter diffraction and the mechanical properties were studied by uniaxial tensile tests, Charpy impact tests and hardness measurements. The passivation behaviour was analysed using the electrochemical potentiodynamic reactivation, whereas the pitting corrosion resistance was compared by pitting potentials and pitting temperatures. However, secondary thermal influences or suboptimal heat treatment can impair the corrosion resistance due to the precipitation of secondary phases and the resulting sensitisation. Thermodynamic calculations and artificial ageing treatment in the range of 500–900°C for up to 100 h were used to determine critical time–temperature parameters for sensitisation. The microstructure of the various aged states was evaluated by scanning electron microscopy and compared with the degrading corrosion resistance characterised by the KorroPad method.

KEYWORDS

ageing, austenitic stainless steel, corrosion resistance, electrochemical methods, high-nitrogen steel, mechanical properties, sensitisation

1 | INTRODUCTION

Nickel-free, austenitic high-nitrogen-alloyed stainless steels, so-called AHNS, such as P2000 (X13CrMnMoN18-14-3), are a relatively young class of materials. The austenitic phase in these alloys is stabilised with a high alloy content of

manganese and nitrogen.^[1] One problem that limits the wider use of these alloys, however, is the limited nitrogen solubility in the steel melt (approximately 0.3 wt%) at atmospheric pressure (1 bar).^[2] Therefore, complex manufacturing processes, such as pressure electroslag remelting, in a nitrogen overpressure atmosphere between 4 and 8 bar

This is an open access article under the terms of the [Creative Commons Attribution License](https://creativecommons.org/licenses/by/4.0/), which permits use, distribution and reproduction in any medium, provided the original work is properly cited and is not used for commercial purposes.

© 2021 The Authors. *Materials and Corrosion* published by Wiley-VCH GmbH

must be used to realise nitrogen contents of approximately 0.8 wt%.^[3,4] Despite this challenging and expensive method, the mechanical properties and achievable corrosion resistance justify the expenses of such a complex manufacturing process.^[4,5] The nitrogen (0.8 wt%) dissolved in the solid solution significantly increases the strength of austenite without reducing its ductility or toughness.^[1,6–9] At the same time, the alloyed nitrogen improves the pitting and crevice corrosion resistance.^[10,11] In addition, some high-nitrogen austenitic stainless steels, such as the P900N Mo and P2000, contain 2–3 wt% molybdenum, which facilitates passivation in acids, improves passive layer stability and, thus, significantly enhances the corrosion resistance.^[5,10,12,13]

It has been proven that the optimum corrosion resistance of stainless steels is achieved under solution-annealed conditions. In this state, the alloying elements, in particular chromium, molybdenum and nitrogen, are homogeneously distributed in the austenitic matrix, which enables the material to build a corrosion-resistant passive layer. In addition, the solution-annealed condition guarantees that the microstructure is free of secondary phases, such as Cr_2N , M_{23}C_6 and σ -phase.^[14–17] The formation of chromium-rich precipitates binds chromium or molybdenum and locally depletes the chromium from the surrounding local matrix.^[18,19] Such locally depleted areas represent a weak link of the passive film and impair the corrosion resistance.^[14,15,17]

The breakdown of the passive layer and the associated reduction in the corrosion resistance due to the chromium-depleted zones is referred as sensitisation. Both the degree of sensitisation and the resulting susceptibility to localised corrosion generally increase with the secondary phase fraction.^[14,15,20] At the same time, the continuous formation of precipitates reduces the toughness of the material to the point of brittle fracture.^[9,21] However, the Charpy impact energy decreases only when the majority of the grain boundaries are continuously covered with precipitates. This requires more diffusion processes than the formation of chromium-depleted areas.

Secondary phases may be formed under the additional influence of heat during its service or during the manufacturing process. Both the temperature and time necessary for the formation of secondary phases as well as the extent of the property changes depend on the exact chemical composition of the material.^[10,14,15,17] Studies on various nitrogen-containing austenites have shown that sensitisation, due to the formation of Cr_2N , tends to occur in the temperature range from 500°C to 1000°C (Figure 1) and that an increase in the nitrogen content causes sensitisation to start earlier and with lower temperature.^[11] The formation of chromium-rich carbides of the M_{23}C_6 type can also occur in the temperature range

from 400°C to 800°C if, in addition to nitrogen, a sufficient amount of carbon is dissolved in the austenite.^[22] It should be noted, however, that stabilisation by stronger carbide formers, such as Zr, Ti, Ta or Nb, does not make sense for nitrogen-alloyed austenites, as nitrogen would then preferentially form corresponding nitrides.

In line with previous research, Figure 1 suggests that the high nitrogen content of pressurised steels, such as P2000, causes this alloy to be susceptible to sensitisation.^[11] However, to the best of our knowledge, no studies have focused on the influence of different molybdenum and manganese contents on the sensitisation tendency. Molybdenum reduces the diffusion rate in austenites, whereas manganese increases the temperature-dependent solubility of nitrogen in solid solutions.^[1,9,11] Owing to this deviation from currently known systems, an exact characterisation of the sensitisation behaviour is essential for the safe use of the new material P2000 (X13CrMnMoN18-14-3).

The properties of the newly developed P2000 (X13CrMnMoN18-14-3) are not yet sufficiently known in the solution-annealed state. However, to make use of the full potential of the material and, at the same time, determine the possible application limits with regard to its sensitisation tendency, solution-annealed samples were first extensively characterised in terms of mechanical properties and corrosion resistance. For better classification, the results of this investigation were compared with the properties of established nickel austenites, such as 304 (1.4301) and 316 (1.4404). Subsequently, the sensitisation tendency of the P2000 was investigated to determine possible processing and application temperatures. For this purpose, solution-annealed samples were sensitised by defined isothermal annealing tests and changes in the microstructure and corrosion resistance were comprehensively characterised.

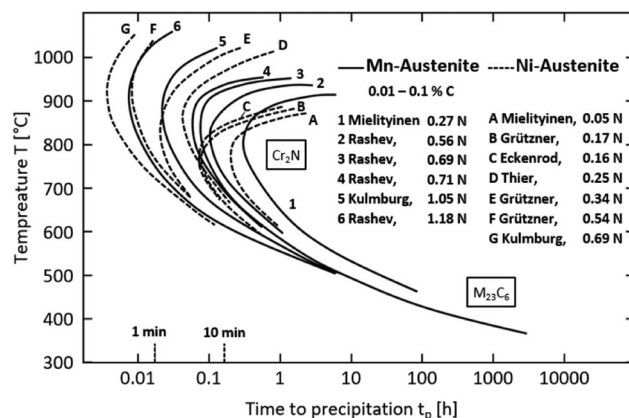


FIGURE 1 Time-temperature transformation diagram of several nitrogen-alloyed austenitic stainless steels. Reproduced with permission.^[11] 1990, Harzenmoser

2 | MATERIALS AND METHODS

2.1 | Materials and heat treatment

First, the investigated alloy of P2000 was produced using a pressure electroslag remelting (P-ESR-process) process by Energietechnik Essen GmbH. Then, 4-mm-thick discs were cut out of a single rod-shaped semi-finished product with a diameter of 50 mm and then cut in half, yielding a semi-cylindrical final sample geometry. The sample geometry of the nickel austenites included rectangles (25 × 50 mm) cut by a laser from thick sheets of 2.5 (304) or 3.0 mm (316). All samples were produced from a single batch of material to guarantee comparability. Table 1 shows the chemical compositions of the materials used.

The nickel-containing austenites 304 and 316 were solution-annealed at 1050°C for 30 min and quenched in water to guarantee a homogeneous condition for the following characterisation. The resulting oxide layer was removed from all sides by wet grinding with SiC paper (80-grit).

The CALCulation of PHase Diagrams method uses thermodynamic and property databases in conjunction with extrapolation methods for the descriptions of binary and ternary systems to higher order systems. This allows the calculation of data for higher order systems that are still unknown. Using this method, the corresponding phase fraction of P2000 occurring in thermodynamic equilibrium was calculated (Figure 2). For this purpose, the software ThermoCalc with the database TCFe10 and the chemical compositions shown in Table 1 were used.

Figure 2 shows a decrease in the phase fraction of the existing precipitation phases (Cr_2N , M_6C , M_{23}C_6 , Laves and σ phase) between 500°C and 1050°C. Above 1050°C, all chromium-rich phases dissolve into a single-phase austenitic solid solution. To guarantee the dissolution of all secondary phases and reduce the necessary holding time, samples of P2000 were solution-annealed at 1150°C for 15 min under atmospheric conditions and quenched in water (20°C). This solution-annealed condition was characterised in terms of its properties and forms the basis for the subsequent ageing tests to determine the sensitisation behaviour. The temperatures and times selected for the annealing tests

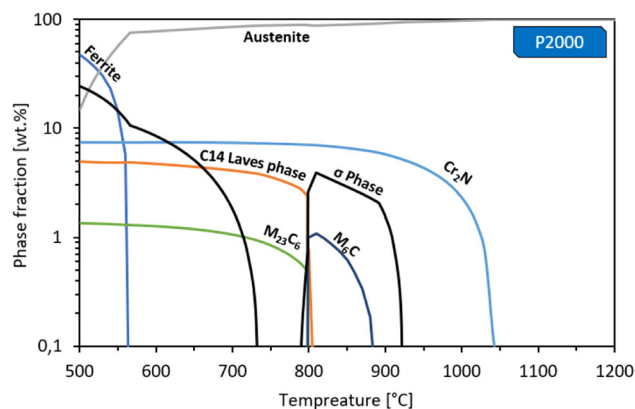


FIGURE 2 Phase diagram of P2000 (X13CrMnMoN18-14-3) calculated, for the sample composition, with ThermoCalc (database TCFe10) [Color figure can be viewed at wileyonlinelibrary.com]

were chosen on the basis of the ThermoCalc simulation in the temperature range from 500°C to 900°C and are summarised in Table 2.

After each heat treatment step, the samples were quenched in water to cool them down to room temperature and prevent further unintentional precipitation. After the last heat treatment step, the oxide layer formed during the heat treatment process was removed from all sides by grinding with SiC paper (80-grit) under continuous water cooling. At the end, at least 0.5 mm of the surface to be examined was ground off to eliminate the influence of edge denitriding and decarburisation on the examinations.

2.2 | Investigation of the microstructure and mechanical properties

The microstructures of all listed conditions were imaged with a DualBeam FEI Scios system (FEI) using secondary electron contrast. During the preparation process, the samples were first ground using SiC abrasive paper with increasing grit size (80/180/360/600/1200/2400) under continuous water cooling, then polished using 3- and 1- μm diamond suspension and finally etched with Beraha II (800 ml of distilled water, 400 ml of hydrochloric acid, 48 g of ammonium hydrogen difluoride and 1 g potassium disulfite) for about 30 s.

TABLE 1 Chemical compositions (wt%) of P2000 (X13CrMnMoN18-14-3), 304 (X5CrNi18-10) and 316 (X2CrNiMo17-12-2)

		C	Cr	Mn	Mo	N	Ni	P	S	Fe
304	X5CrNi18-10	0.025	18.8	1.5	0.2	0.06	8.2	0.023	0.003	Bal.
316	X2CrNiMo17-12-2	0.023	17.6	1.0	2.0	0.03	10.2	0.020	0.001	Bal.
P2000	X13CrMnMoN18-14-3	0.07	16.2	12.8	3.2	0.82	0.11	0.015	0.007	Bal.

TABLE 2 Ageing parameters of the created samples

Temperature	Ageing time							
	10 min	1 h	5 h	10 h	20 h	50 h	100 h	
500°C								
600°C	5 min	10 min	30 min	1 h	2 h	4 h	8 h	
700°C	1 min	5 min	10 min	30 min	1 h	2 h	4 h	
800°C	1 min	5 min	10 min	30 min	1 h	2 h	4 h	
900°C	1 min	5 min	10 min	30 min	1 h	2 h	4 h	

For the final observation of the solution-annealed states by means of electron backscatter diffraction (EBSD) using the FEI Scios DualBeam, the samples were cut under continuous water cooling, conductively embedded, wet-ground with increasing grain size (maximum 2400) and polished with 3- and 1- μm diamond suspension. Finally, the samples were finished on a vibratory polisher with the following parameters: Eposil M11 and distilled water (1:1), 6 h, one additional weight per sample (200 g).

One area per sample was scanned with a step size of 1 μm at an accelerating voltage of 20 kV. Kikuchi patterns were recorded using a Hikari EBSD system from EDAX (Ametek GmbH—EDAX Business Unit) along with the associated software TEAM V4.6. Then, the EBSD scans were analysed using TSL OIM Analysis 8. Finally, the EBSD data were postprocessed using neighbour orientation correlation, and the corresponding images were subsequently generated.

To determine the strength and ductility of P2000, the selected conditions were investigated by an uniaxial tensile test using a RM250 tensile test rig (Carl Schenk GmbH) with a type ME 53-33 Laser Speckle Extensometer (Doli Elektronik GmbH) in accordance with DIN EN ISO 6892-1:2017 (Method B) at room temperature (20°C).^[23] After the heat treatment, the diameter of the samples in the measurement zone was reduced to 8 mm using a lathe machine to prevent denitration in the near subsurface area of the samples and thus an impact of denitration on the measured material properties. This resulted in a final sample geometry according to DIN 50125.^[24] During the test, the applied force was increased at a rate of 3 kN/min, and the resulting strain (ϵ) was measured at a sampling rate of 50 Hz by means of a M53 strain transducer until the specimen broke. The yield strength ($R_{p0.2}$), tensile strength (R_m) and elongation at break (A5) were then determined.

As Supporting Information Data, the toughness of the solution-annealed specimens was investigated at room temperature using the Charpy-V notched bar impact test. In addition, the influence of sensitisation was characterised by investigating the change in the Charpy

impact energy of the selected conditions as compared with the solution-annealed states. For this purpose, the V-notch geometry standardised in DIN EN ISO 148-1 was used.^[25]

2.3 | Corrosion investigations

Electrochemical potentiodynamic reactivation (EPR) was used to determine the maximum passivation current density (I_p) and reactivation current density (I_r). Generally, I_p shows how P2000 passivates under the given conditions as compared with nickel-containing stainless austenites, whereas I_r indicates whether the passive layer formed during anodic polarisation is sufficiently resistant under the test conditions. Potentiodynamic measurements were performed with a PS6 potentiostat from Meinsberg (now: Sensortechnik Meinsberg—Xylem) using a classical three-electrode arrangement: an Ag/AgCl reference electrode (ESHE = +197 mV), a platinum counter electrode and the samples as the working electrode.

Before the measurement, the sample surfaces were wet-ground with 600-grit SiC paper, cleaned with distilled water and isopropanol and dried under a stream of warm air. Then, a silicone ring and a plexiglass measuring cell ($\varnothing_{\text{inside}} = 14 \text{ mm}$) were immediately positioned on the sample, fixed by a mechanical clamping device, and placed within the measuring setup. The used measurement parameters were in line with ASTM G108, which describes the standard test method for EPR for detecting sensitization of AISI Type 304 and 304 L Stainless Steels.^[20] So, the measuring cell was filled with test electrolyte (0.5 M H_2SO_4 + 0.01 M KSCN) and the measurement was started. As a first step of the measurement, the samples were passivated using anodic polarisation with a sweep rate of 2 mV/s, starting from $-500 \text{ mV}_{\text{Ag/AgCl}}$ up to the reverse potential ($+300 \text{ mV}_{\text{Ag/AgCl}}$). Then, the polarisation direction was reversed, followed by polarisation with 2 mV/s in the cathodic direction (reactivation) until the initial potential ($-500 \text{ mV}_{\text{Ag/AgCl}}$) was reached.

To quantitatively compare the pitting corrosion resistance values of the investigated alloys, the critical

pitting corrosion potential at 50°C (E_{pit}) and critical pitting corrosion temperature (CPT) were determined according to ASTM G150^[26] and ASTM G48,^[27] using continuous heating of the test solution and electrochemical noise measurements to detect the transition to stable pitting. In preparation for these measurements, the samples were first wet-ground on all sides with 180-grit paper and then the edges were broken with 1000-grit paper, cleaned and dried. Next, the samples were stored inside a glass container with more than 95% relative humidity, monitored using a hygrometer, for 24 h. Such deposition enables the formation of a durable passive layer on the surface of the samples. After the passivation process, a welding wire was spotted on the face side of the passivated sample for electrical contact.

To determine the critical pitting corrosion potentials, the sample was then immersed in the test electrolyte (0.1 M NaCl borate buffer solution, pH 7.1) until an effective measuring area of 5 cm² was realised. To prepare for the experiment, approximately 400 ml of the electrolyte was tempered in a double-walled measuring cell from Meinsberg to 50°C using a Julabo HD-4 thermostat (JULABO GmbH) before the experiment. The sample was then contacted as a working electrode, resulting in a classical three-electrode measuring arrangement with a platinum counter electrode and an Ag/AgCl reference electrode. Finally, measurement was carried out with a Gamry Interface 1000 (Gamry Instruments), in which the resting potential of the sample was first determined for 10 min. Starting from the determined resting potential after 10 min, the sample surface was then polarised at 1 mV/s in the anodic direction until pitting corrosion started and the current density exceeded a value of 0.3 mA/cm² or the transpassive region was reached. The critical pitting potential was then determined at the value when the current density permanently exceeded a value of 0.1 mA/cm².

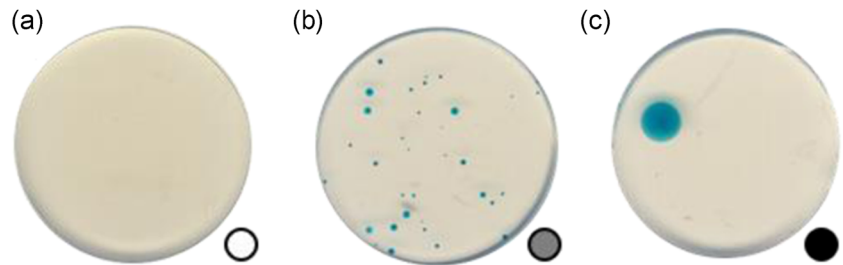
To determine the CPT according to ASTM G150, the prepared and passivated sample was positioned in the measuring setup, analogous to the determination of E_{pit} . Therefore, a measuring area of 5 cm² inside the 400 ml electrolyte (1 M NaCl, 58.44 g/L), preheated to 10°C with a thermostat (Julabo HD-4), was realised. The measurement was then performed using a three-electrode arrangement, in which the actual reference electrode element was located outside the measuring cell and kept at room temperature (22°C) to prevent temperature-related fluctuations in the reference potential. For the test, the sample was anodically polarised at a fixed potential of +745 mV_{Ag/AgCl} using a Gamry Interface 1000 potentiostat and the temperature was increased from 10°C at a heating rate of approximately 1 K/min according to the standards. Due to the inertia of the

thermostat used and the high heating rate required, it took about 4 min for the temperature of the test solution to rise linearly. The temperature was increased until stable pitting corrosion was initiated, and the current density exceeded a value of at least 0.2 mA/cm². Determination of the CPT was then performed according to ASTM G150^[26] at the temperature at which permanent exceeding of a current density value of 0.1 mA/cm² was detected.

The CPT in accordance with ASTM G48 (Method A)^[27] was determined with the help of electrochemical noise. The setup used can be traced back to the work of Heyn and Goellner.^[28] In this method, two similarly prepared and passivated samples of the material to be tested are immersed in a standardised test solution (6 wt% FeCl₃) and exposed to the solution at 10 K below the theoretical critical temperature for 1 h.^[27] Then, the temperature is continuously increased at a rate of 10 K/h and the electrochemical current noise is measured. A zero-resistance ammeter (ZA-01/ZU-01; IPS-Ingenieurbüro Schrems) was used for this purpose. Then, the current noise is separated from the DC component by a high-pass filter and then low-pass-filtered and amplified. The effective frequency range of the measurement signals is between 0.1 and 10 Hz, with an amplification factor of 100. The transition from metastable to stable pitting corrosion is recognisable from the clearly increased intensity and duration of the current noise signals, allowing the test to be terminated after stable pitting corrosion is reached. The temperature at which the transition to stable pitting corrosion occurs is calculated subsequently from the measurement data. For this purpose, any offset is removed from the data and the current noise signals are rectified and integrated. This results in a charge-temperature curve with two characteristic areas. The initial passive and metastable state has a flat slope, whereas the state of stable pitting corrosion has a steep one. By linear interpolation of the curve for each of the two characteristic ranges, their intersection point can be determined, which is defined as the critical pitting temperature.

To characterise the influence of sensitisation on P2000 as quickly and effectively as possible, the precipitation behaviour was observed and the change in the pitting corrosion resistance was detected using the KorroPad method. First invented in 2014, this relatively new method has been successfully used for this purpose on stainless austenitic, martensitic and duplex steels.^[14,15,29–32] During the preparation process, the samples were wet-ground with 180-grit SiC paper, cleaned, dried in warm air and passivated at more than 95% relative humidity. For the experiment, KorroPads with a composition of 0.1 M NaCl and 1 mM K₃[Fe(CN)₆] and a diameter of 20 mm were placed on

FIGURE 3 Typical results of KorroPad testing: (a) no blue spots \approx stable passive layer; (b) small blue spots \approx metastable pitting corrosion (with repassivation); (c) one large blue spot \approx stable pitting corrosion (without repassivation) [Color figure can be viewed at wileyonlinelibrary.com]



the surface for 15 min. Through the placement of the KorroPad, the passive sample surface was anodically polarised to $+275 \text{ mV}_{\text{Ag}/\text{AgCl}}$ and corrosively loaded by a combination of $\text{K}_3[\text{Fe}(\text{CN})_6]$ and NaCl , which are dissolved inside the Agar-gel matrix of the pad. If pitting corrosion is initiated, the iron cations released during the dissolution process react with $\text{K}_3[\text{Fe}(\text{CN})_6]$, which translates into a Prussian-blue colour in the gel pad. Both the degree of pitting corrosion that occurred and the correlating pitting corrosion resistance of the differently sensitised states were visually evaluated according to Figure 3.

3 | RESULTS AND DISCUSSION

3.1 | Comparison of solution-annealed properties

Figure 4 compares the microstructures in the solution-annealed condition of the two Cr–Ni austenites 304 and 316 with the microstructure of the Cr–Mn–N austenite P2000.

As expected, all materials showed a single-phase austenitic microstructure.^[1] This was confirmed by the EBSD scans in which the austenitic phase was indicated with a high confidence index in all the samples. At the same time, the average grain size was determined from the EBSD scans. At this point, it should be noted that this

size was smaller than the real size due to the systematic error that arises as the software also evaluates the grains in the edge area of the scan. Despite this, the qualitative effect could still be observed. Evaluation of the average grain size in Figure 4 shows that P2000 exhibits a significantly larger grain size than those of 304 and 316. This is due to the higher solution annealing temperature (1150°C) of P2000, which, according to the thermodynamic calculations (Figure 2), is required to dissolve the nitrides (Cr_2N) and establish a homogenous distribution of the 0.8 wt% nitrogen in the austenitic matrix.

While no further significant differences between the three alloys were evident in the microstructure, the mechanical properties of the different alloy concepts (Cr–Ni vs. Cr–Mn–N) widely differed. Thus, the characteristic values of the determined σ – ϵ diagram of P2000 (Figure 5) prove a significantly higher strength than that of nickel austenites 304 and 316 with comparable ductility. Such higher strength of P2000 is attributed to the mechanism of solid solution strengthening because the entire nitrogen content (0.8 wt%) is forcibly dissolved in the solid solution. This also explains why the hardness of solution-annealed P2000 (i.e., 280 HV10) is significantly higher than that of 304 or 316 with a maximum of 215 HV10. It is also possible to further increase the tensile strength of P2000 to $R_m = 1800 \text{ MPa}$ by work hardening.^[5] A comparison of the deformation behaviour shows that P2000 with 53% A5 elongation and an impact energy of greater

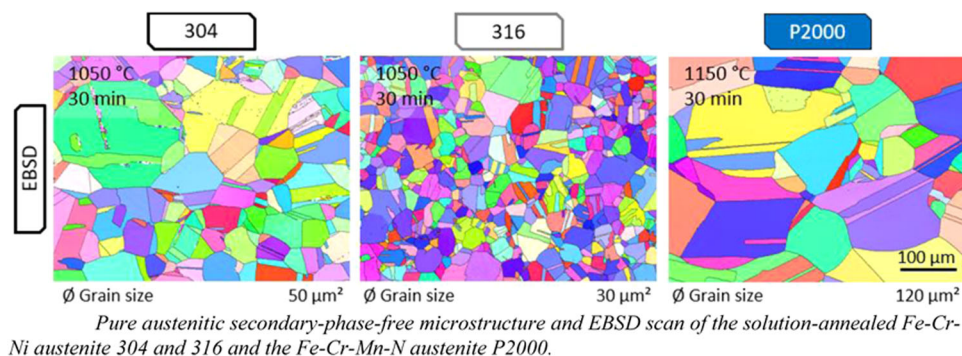


FIGURE 4 Pure austenitic secondary-phase-free microstructure and EBSD scan of the solution-annealed Fe–Cr–Ni austenite 304 and 316 and the Fe–Cr–Mn–N austenite P2000. EBSD, electron backscatter diffraction [Color figure can be viewed at wileyonlinelibrary.com]

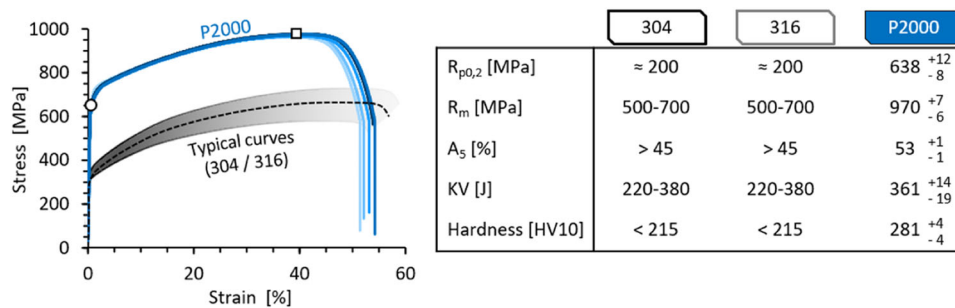


FIGURE 5 The determined σ - ϵ diagram of solution-annealed P2000, with the resulting characteristic and hardness values (HV10) in comparison to the literature values of 304 and 316^[33-38] [Color figure can be viewed at [wileyonlinelibrary.com](#)]

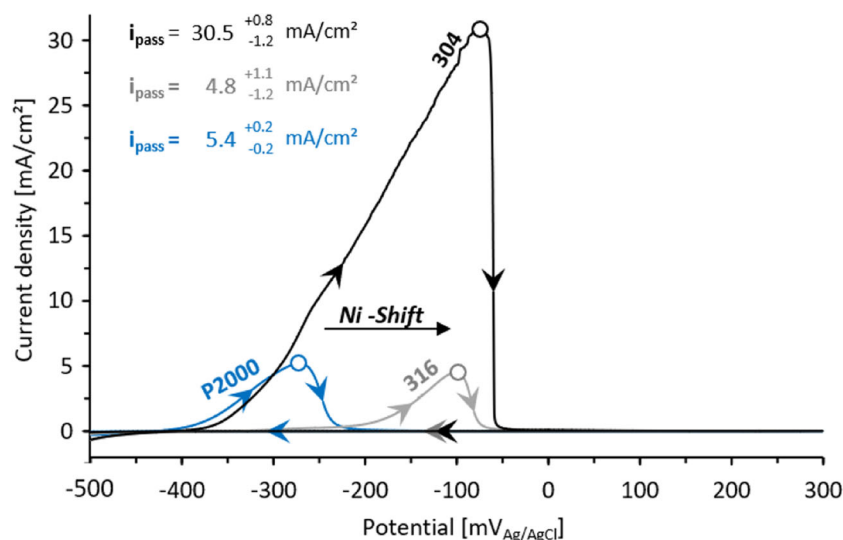


FIGURE 6 Measured electrochemical potentiodynamic reactivation curves and resulting passivation current density of solution-annealed 304, 316 and P2000 [Color figure can be viewed at [wileyonlinelibrary.com](#)]

than 361 J is comparable to common nickel austenites.^[33-37] This is due to the single-phased austenitic microstructure and resulting face-centred cubic crystal lattice structure in all the samples.

The following section shows a comparison of the corrosion resistance property of stainless steel P2000 with common Cr-Ni austenites, which is the second core feature of these materials. Figure 6 shows typical curves for the EPR measurements of the solution-annealed states and the resulting passivation current densities.

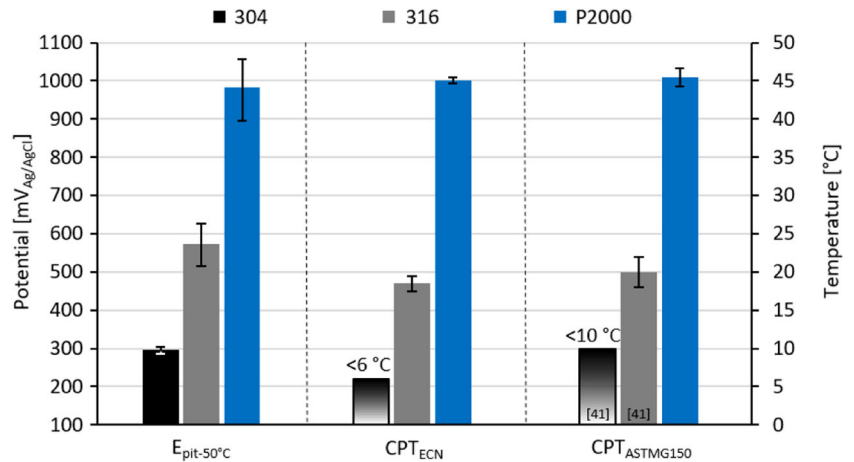
Although nickel increases acid resistance,^[39,40] the passivation current density of nickel-free P2000 (5.4 mA/cm²) was found to be comparable to the 316 and significantly lower than that of the 304. This is due to the 3 wt% molybdenum, which is homogeneously dissolved in the solid solution of P2000 in the solution-annealed state and decreases the necessary i_p . As a result, P2000 has 1 wt% more molybdenum than 316, which explains the comparable passivation current densities despite the lack of nickel. At the same time, this is further emphasised by the massive difference of the i_p from 304 with no

significant molybdenum content. In addition, a reduction was observed in the potential necessary for passivation from -60 ± 23 mV_{Ag/AgCl} (304) and 89 ± 12 mV_{Ag/AgCl} (316) to -270 ± 7 mV_{Ag/AgCl} for the nickel-free P2000. During repolarisation, no renewed increase was observed in the current density for any of the three steels. The absence of reactivation proves that the solution annealing process served its purpose, and the passive layers formed during anodic polarisation were found to be resistant, with no detectable weak points in the microstructure (e.g., chromium depletion). This means that the alloying elements relevant to corrosion resistance, especially chromium and molybdenum, were homogeneously distributed in the solid solution.

Figure 7 summarises the results for determining the pitting corrosion resistance of the three solution-annealed stainless steels by critical pitting potentials at 50°C and by the CPT values.

The ranking of the determined pitting corrosion resistance for 304, 316 and P2000 was found to be the same for all three methods. Thus, 304 has the lowest pitting corrosion resistance, 316 has slightly higher pitting

FIGURE 7 Critical pitting potentials at 50°C and the CPT measured with electrochemical noise and according to ASTM G150 of solution-annealed 304, 316 and P2000.^[41] CPT, critical pitting corrosion temperature [Color figure can be viewed at wileyonlinelibrary.com]



corrosion resistance and the still relatively unexplored P2000 clearly has the highest one, which can be readily observed in the values of E_{pit} and CPT_{ASTM G150/ECN}. In general, there are three alloy-related reasons for the excellent pitting corrosion resistance of P2000. First, P2000 is alloyed with an extremely high nitrogen content of 0.8 wt%. This massively increases the pitting corrosion resistance as compared with conventional austenitic stainless steels with nitrogen content less than 0.1 wt%.^[10,11] Second, P2000 contains about 3 wt% molybdenum, which further increases the pitting corrosion resistance.^[10,13] This effect is again further illustrated by comparing the molybdenum-containing 316 (2 wt%) with the molybdenum-free 304 (0.2 wt%). Third, among the class of Cr–Mn–N austenites, P2000 has a comparatively small content (13 wt%) of manganese, which lowers the pitting corrosion resistance of stainless steels.^[10,13] However, the tendency to form chromium-rich precipitates is of great importance for the heat treatment,

manufacturing process and application of P2000. As manganese increases nitrogen solubility^[1,11] and the high nitrogen content influences the sensitisation behaviour, an experimental study is necessary to evaluate the processing and application window.

3.2 | Sensitisation behaviour of P2000

As secondary phase formation can negatively influence the mechanical properties and corrosion resistance of stainless steels, the kinetics of precipitation and the associated sensitisation behaviour should be known for safety purposes. Figure 8 shows the experimentally determined time–temperature precipitation diagram, which summarises the effects of ageing within the temperature range from 500°C to 900°C on the microstructure of P2000. The possible microstructures are divided into three categories, which are illustrated by exemplary

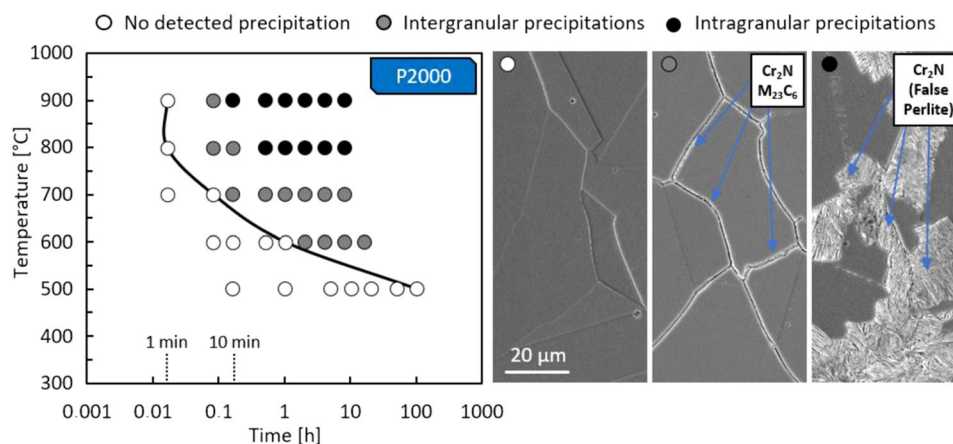


FIGURE 8 Time–temperature precipitation diagram, based on scanning electron microscopy micrograph, showing the formation of $Cr_2N/M_{23}C_6$ and false Cr_2N perlite as a result of the isothermal ageing of P2000. The figure shows examples for microstructures without precipitation as well as intergranular and intragranular precipitation to clarify the evaluation criteria [Color figure can be viewed at wileyonlinelibrary.com]

scanning electron microscopy micrographs of the typical microstructures during sensitization.

The black line in Figure 8 separates the precipitation-free temperature–time (T–t) region from the T–t region with visible precipitates within the microstructure. The results show that an increase in the temperature and the corresponding higher diffusion rates reduce the necessary ageing duration until the first formation of precipitates. Thus, no secondary phases were detected by SEM after ageing at 500°C, even after 100 h. Starting from 600°C, the first precipitates were detected at the grain boundaries after 1 h, at 700°C after 10 min and at $\geq 800^\circ\text{C}$ after 5 min. These precipitates resulted from the high supersaturation of the austenite solid solution with nitrogen (0.8 wt%) and carbon (0.07 wt%). According to the thermodynamic calculations in Figure 2, this leads to the possible formation of chromium-rich nitrides and carbides as well as σ and Laves phases between 500°C and 900°C. The results obtained, however, do not prove which of the precipitates, depending on the temperature, forms first. Nevertheless, the dominantly detected secondary phase in the microstructure at all of the investigated ageing temperatures was chromium-rich nitrides of the M_2N type.

At higher temperatures, more and more nitrides occupy the grain boundaries. In addition, starting from 800°C, nitride precipitation occurs in the grain interior. At 800°C, this occurs after 1 h, but at 900°C, it readily occurs after 10 min. As shown in Figure 9, as the artificial ageing time increases, the precipitates grow in a lamellar morphology, starting from the grain boundaries into the interior of the austenite grain. The secondary phases, as

shown by the thermodynamic simulations in Figure 2 and in the results of Rosemann et al.,^[32] are primarily Cr_2N . This lamellar arrangement of Cr_2N and austenite is also called false pearlite. The qualitative optically recognisable phase fraction of the secondary phases increases with the ageing time and temperature. The fact that P2000, in comparison to nickel-containing austenites, such as 304 and 316, still shows a massive growth of false pearlite at temperatures of 800°C or 900°C is due to two factors: (1) the high nitrogen content of the P2000 alloy and (2) the 13 wt% manganese content, which is comparatively low for Cr–Mn–N austenite. This increases the tendency of nitrides to precipitate, as it causes P2000 to have reduced nitrogen solubility as compared with a typical Cr–Mn–N austenite with a content of 18 wt% manganese. This is particularly noticeable when comparing the precipitation behaviour at 900°C between P2000 and P900N + Mo.^[32]

During the formation of the chromium-rich secondary phases, which are visible in the microstructure (Figures 8 and 9), both chromium and, possibly, molybdenum are removed from the surrounding austenitic matrix. This results in alloy-element-depleted areas at the transition zone between secondary phases and matrix. Therefore, the corrosion resistance is expected to be impaired by the formation of secondary phases. Figure 10 summarises the results of the KorroPad test for the different artificial ageing conditions and shows the influence of secondary phase formation on the pitting corrosion resistance.

The results show that artificial ageing significantly reduced the pitting corrosion resistance. Analogous to the initial formation of secondary phases in the

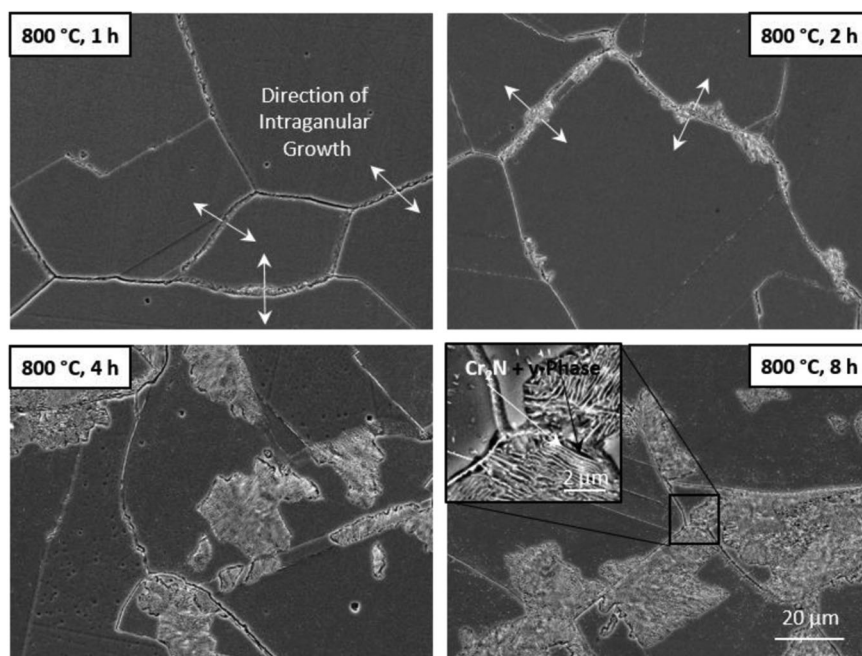


FIGURE 9 Scanning electron microscopy micrograph of the intragranular growth of lamellar Cr_2N ('false pearlite') after ageing at 800°C for 1–8 h

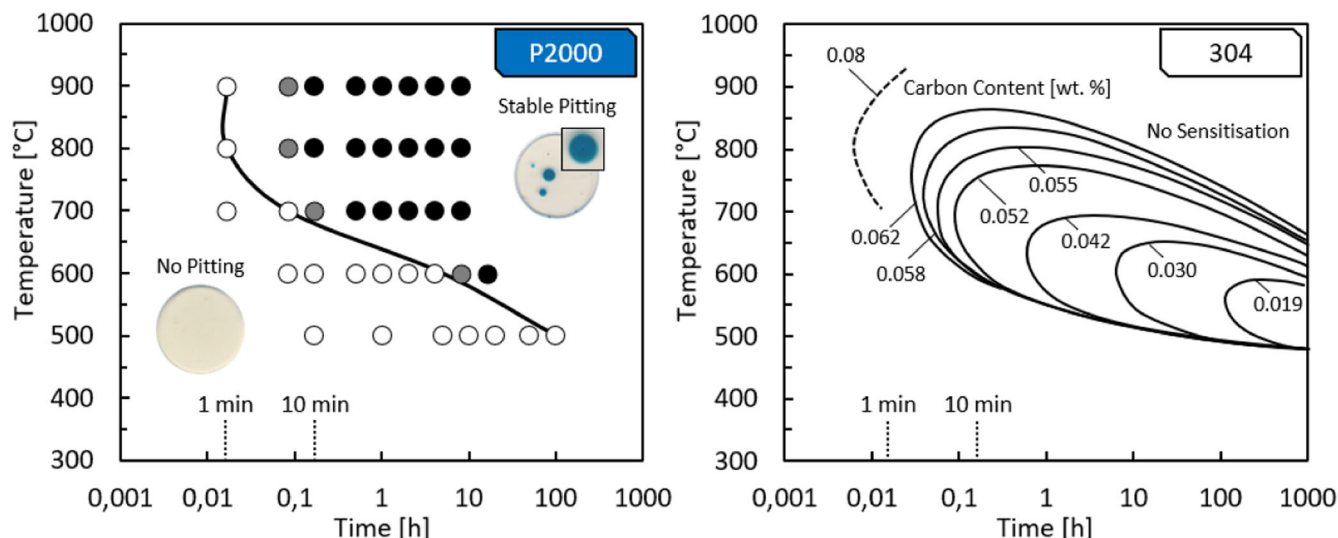


FIGURE 10 Determined sensitisation diagram, based on the KorroPad indication test, for the reduction of the pitting resistance due to ageing in comparison to the sensitisation behaviour of nickel-containing 304, depending on the carbon content^[22] [Color figure can be viewed at wileyonlinelibrary.com]

microstructure (Figure 8), the time required for this process decreases with increasing temperature. The black line in Figure 10 corresponds to the resulting sensitisation curve of P2000. This shows temperatures and ageing times at which the pitting corrosion resistance of P2000 is significantly reduced. Comparison of the determined sensitisation curve (Figure 10) with the times of the first precipitation in the structure (Figure 8) reveals an absolute agreement at 500°C and from 700°C to 900°C. At 600°C, the corrosion resistance decreases only after an artificial ageing period of 8 h; however, the precipitation was already detected in the grain boundaries after 1 h. A possible explanation for this is that the chromium depletion after less than 8 h of ageing was limited and local enough that these areas were dissolved during the 24-h passivation. This process would allow the material to still build up a protective passive layer.

Direct comparison of the initial sensitisation of P2000 between 500°C and 800°C shows a good correlation with the idealised sensitisation curves of nickel austenites with a higher carbon content (≤ 0.06 wt%), such as 304. However, the fact that P2000 has a comparatively high carbon content of 0.07 wt% is considered to be unfavourable because the kinetically preferred secondary phases of $M_{23}C_6$ carbides and M_2N nitrides can form simultaneously. Therefore, future research should clarify whether the initial sensitisation of P2000 results from the formation of chromium-rich carbides or nitrides. Nevertheless, according to the thermodynamic calculations (Figure 2 at higher temperatures (i.e., above 800°C), the effect of the decreasing pitting resistance can be readily attributed to the formation of Cr_2N , as carbon is still dissolved in the austenite.

Over the entire characterised parameter range, it can be observed that the corrosion resistance of the P2000 is further reduced with increasing secondary phase fraction in the microstructure. This leads so far that in contrast to nickel-containing austenites, such as 304, no desensitisation (i.e., renewed improvement in the pitting corrosion resistance) was determined even after a long time at high temperatures (900°C, 10 h). Hence, it can be seen that Cr_2N precipitation, which was due to the high nitrogen and low manganese content, was so strong that at 800°C and 900°C, a significant content of chromium and nitrogen was bound. As a result, even with the rediffusion of chromium and nitrogen from the matrix into the depleted zones, the corrosion resistance could not be decisively improved. In the case of standardly used nickel austenites, such as 304, permanent significant sensitisation is not possible at high temperatures ($\geq 800^\circ C$) due to the low carbon (≥ 0.06 wt%) and nitrogen content.^[22]

It should be noted that the strong precipitation in P2000 results not only in a reduction in the pitting corrosion resistance but also in a massive reduction in the Charpy impact energy. This critical safety value was reduced from 361 ± 15 J in the solution-annealed condition to only 10 ± 2 J after only 1 h at 700°C. Such susceptibility to spontaneous loads in the sensitised condition is extremely critical for the safe use of these materials. Nickel austenites, such as 304 and 316, however, only show a moderate reduction in the impact energy in the strongly sensitised state, compared with the solution-annealed state.^[33] This is because the maximum possible secondary phase content in Fe–Cr–Ni austenites is much lower than that in Fe–Cr–Mn–N austenites due to the different alloying

concepts. Hence, reheating of P2000 above 500°C should be avoided during production, processing and use.

4 | CONCLUSIONS

The results and comparisons presented in this paper make it possible to characterise and classify the properties of the nickel-free Fe–Cr–Mn–N austenite P2000 and compare it with conventional nickel-containing austenites such as 304 and 316. The first point discussed here was the mechanical properties. It was shown that, in the solution-annealed condition, the strength and hardness of P2000 are significantly higher than those of the nickel austenites 304 and 316. However, despite such high strength and hardness of P2000, its ductility and toughness were comparable to those of its conventional counterparts due to the austenitic matrix. Second, the passivation behaviour was characterised by applying the EPR method according to ASTM G108. It was found that the converted charge necessary for passivation or the passivation current density in acidic conditions is comparable to that of the molybdenum-containing nickel austenite 316. At the same time, a shift in the passivation potential of P2000 as compared with nickel-containing austenites was determined. Third, investigations regarding the pitting corrosion resistance by means of E_{pit} and CPT showed that the pitting corrosion resistance of P2000 is significantly higher than that of 304 and 316. According to a CPT ASTM G 48 of approximately 45°C, P2000 is therefore comparable to the austenite 904 L (CPT ASTM G 48 of 40°C) in terms of pitting corrosion resistance and more resistant than the duplex steel 318LN (CPT ASTM G 48 of 35°C).

Finally, both the precipitation and sensitisation behaviour of P2000 were characterised. The results revealed an almost absolute correlation between the time of the first detection of precipitation formation and the first reduction of the pitting corrosion in the KorroPad test. The results also showed a further decrease in the pitting resistance with an increasing secondary phase fraction in the microstructure. The favourable correlation found between the KorroPad results and the microstructure reveals the potential to determine sensitisation diagrams of novel materials highly effectively and sensitively with these screening tests. Comparison of the resulting critical T–t parameters with those of 304 showed a good agreement, especially in the area of the initial sensitisation. In contrast to austenites containing nickel, P2000 did not exhibit desensitisation with further ageing due to healing effects. In addition to the reduction observed in the corrosion resistance, the Charpy impact energy was

reduced to a minimum of 10 J by artificial ageing and C₂N precipitation. Such a decrease is critical for future component safety and should be considered in future use scenarios. Therefore, renewed heating of P2000 above 500°C should be avoided as far as possible during production, processing and use. If this is not possible, then a final solution annealing should be performed before use to ensure optimal corrosion resistance and toughness. In summary, if sensitisation during use can be ruled out, then P2000 can be considered superior to conventional austenites in terms of mechanical properties and corrosion resistance.

ACKNOWLEDGEMENTS

Dr. Heyn would like to thank the German Research Foundation (DFG) for funding the project ‘Agar-based gel-electrolytes for corrosion diagnostic’ (project number 330472124). Access funding enabled and organized by Projekt DEAL.

CONFLICT OF INTERESTS

The authors declare that there are no conflict of interests.

DATA AVAILABILITY STATEMENT

The data that support the findings of this study are available from the corresponding author upon reasonable request.

ORCID

Norman Kauss  <http://orcid.org/0000-0002-1852-0376>

Andreas Heyn  <http://orcid.org/0000-0002-0146-219X>

REFERENCES

- [1] P. J. Uggowitzer, R. Magdowski, M. O. Speidel, *ISIJ Int.* **1996**, *36*, 901.
- [2] H. Feichtinger, G. Stein, *Mater. Sci. Forum* **1999**, *261*, 318.
- [3] H. Berns, *Steel Res.* **1992**, *63*, 343.
- [4] V. G. Gavriljuk, H. Berns, *High Nitrogen Steels. Structure, Properties, Manufacture, Applications*, Springer, Berlin, Heidelberg **1999**.
- [5] *Energietechnik Essen, Material Data Sheet P 900 N – P 900 N Mo – P 2000*, **2012**.
- [6] P. J. Uggowitzer, M. O. Speidel, presented at *STAINLESS STEELS '91*, Chiba, Japan, June 10–13, **1991**, p. 762.
- [7] J. W. Simmons, *Mater. Sci. Eng., A* **1996**, *207*, 159.
- [8] S. Koch, R. Büscher, I. Tikhovski, H. Brauer, A. Runiewicz, W. Dudzinski, A. Fischer, *Materialwiss. Werkstofftech.* **2002**, *33*, 705.
- [9] A. A. Rechsteiner, *Ph.D. Thesis*, ETH Zürich (Switzerland) **1994**.
- [10] K. H. Lo, C. H. Shek, J. K. L. Lai, *Mater. Sci. Eng., Rep.* **2009**, *65*, 39.
- [11] M. A. E. Harzenmoser, *Ph.D. Thesis*, ETH Zürich (Switzerland) **1990**.
- [12] P. Rosemann, T. Müller, M. Babutzka, A. Heyn, *Mater. Corros.* **2015**, *66*, 45.

- [13] A. Pardo, M. C. Merino, A. E. Coy, F. Viejo, R. Arrabal, E. Matykina, *Corros. Sci.* **2008**, *50*, 780.
- [14] N. Kauss, A. Heyn, T. Halle, P. Rosemann, *Electrochim. Acta* **2019**, *317*, 17.
- [15] P. Rosemann, C. Müller, N. Kauss, T. Halle, *HTM, J. Heat Treat. Mater.* **2017**, *72*, 87.
- [16] N. Lopez, M. Cid, M. Puiggali, *Corros. Sci.* **1999**, *41*, 1615.
- [17] Z. Zhang, H. Zhao, H. Zhang, Z. Yu, J. Hu, L. He, J. Li, *Corros. Sci.* **2015**, *93*, 120.
- [18] S. M. Bruemmer, L. A. Charlot, *Scr. Metall.* **1986**, *20*, 1019.
- [19] E. L. Hall, C. L. Briant, *Metall. Trans. A* **1984**, *15*, 793.
- [20] ASTM International, *Technical Standard ASTM G108-15*, ASTM International, West Conshohocken, PA **2015**.
- [21] E. Erisir, *Ph.D. Thesis*, RWTH Aachen (Aachen, Germany) **2009**.
- [22] NiDI, *Designers' Handbook Series No. 9014*. The Nickel Institute, Durham, North Carolina **2020**.
- [23] ISO, *Technical standard ISO EN ISO 6892-1*, 2019. <https://www.iso.org/>
- [24] DIN, *Technical standard DIN 50125:2016-12*, **2016**, Beuth Verlag GmbH, Berlin.
- [25] ISO, *Technical standard ISO 148-1:2016*, **2016**. <https://www.iso.org/>
- [26] ASTM International, *Technical standard ASTM G150-18*, **2018**, West Conshohocken, PA.
- [27] ASTM International, *Technical standard ASTM G48-11(2020) e1*, **2020**, West Conshohocken, PA.
- [28] A. Heyn, J. Goellner, *Mater. Corros.* **2007**, *58*, 953.
- [29] P. Rosemann, N. Kauss, WOTECH Kompetenz in Werkstoff und funktioneller Oberfläche **2018**.
- [30] P. Rosemann, N. Kauss, A. Heyn, *IOP Conf. Ser.: Mater. Sci. Eng.* **2020**, *882*, 12017.
- [31] A. Burkert, H. S. Klapper, J. Lehmann, *Mater. Corros.* **2013**, *64*, 675.
- [32] P. Rosemann, C. Müller, T. Halle, *IOP Conf. Ser.: Mater. Sci. Eng.* **2020**, *882*, 12018.
- [33] T. S. Byun, T. Lach, U.S. Department of Energy- Office of Nuclear Energy **2016**.
- [34] Thyssenkrupp Materials Services GmbH, *Material Data Sheet M X5CrNi18-10 1.4301 (304)*, **2018**.
- [35] T. T. H. Le Nguyen, J.-S. Hwang, M.-S. Kim, J.-H. Kim, S.-K. Kim, J.-M. Lee, *Metals* **2019**, *9*, 625.
- [36] Deutschen Edelstahlwerke GmbH, *Material Data Sheet(304), X5CrNi18-10*, **2015**.
- [37] Deutschen Edelstahlwerke GmbH, *Material Data Sheet X5CrNiMo17-12-2 (316)*, **2015**.
- [38] I. Arrayago, E. Real, L. Gardner, *Mater. Des.* **2015**, *87*, 540.
- [39] S. Azuma, T. Kudo, H. Miyuki, M. Yamashita, H. Uchida, *Corros. Sci.* **2004**, *46*, 2265.
- [40] C. Pistorius, M. Du Toit, presented at *The Twelfth Int. Ferrous Alloys Congr. Sustainable Future*, Helsinki, Finland, June 6–9, **2010**, p. 911.
- [41] Outokumpu Stainless AB, *Handbook of Stainless Steel*, Outokumpu Oyj, Avesta, Sweden **2013**.

How to cite this article: N. Kauss, A. Heyn, O. Michael, M. Schymura, P. Rosemann. Application limits and sensitisation behaviour of the manganese- and nitrogen-alloyed austenitic stainless steel P2000 (X13CrMnMoN18-14-3). *Materials and Corrosion*. 2021;72:1656–1667. <https://doi.org/10.1002/maco.202112450>